

**ARTICLE TYPE**

# Enhanced kinematics and distribution characteristics of Upper Scorpius and Ophiuchus associations based on Gaia DR3

W. H. Elsanhoury\*<sup>1,2</sup><sup>1</sup>Physics Department, College of Science, Northern Border University, Arar, Saudi Arabia<sup>2</sup>Astronomy Department, National Research Institute of Astronomy and Geophysics (NRIAG), 11421, Helwan, Cairo, Egypt**Correspondence**

\*W. H. Elsanhoury, Physics Department, College of Science, Northern Border University, Arar, Saudi Arabia.

Email: elsanhoury@nriag.sci.eg &amp; elsanhoury@nbu.edu.sa

**Present Address**

Physics Department, College of Science, Northern Border University, Arar, Saudi Arabia

**Abstract**

The kinematics within the Solar vicinity have revealed interesting features relevant to both stellar and Galactic structures. This study examines three stellar associations in the Upper Scorpius and Ophiuchus regions, along with their sub-samples among Gaia DR3. The calculated kinematics and velocity ellipsoid characteristics, including the mean spatial velocity components ( $U$ ,  $V$ , and  $W$ ; km s<sup>-1</sup>), yielding values of approximately  $(-5.84 \pm 2.42, -16.14 \pm 4.02, -7.31 \pm 2.70)$  km s<sup>-1</sup>. USC and Oph associations velocity dispersion within the ellipsoid ( $\sigma_i$ ,  $\forall i = 1, 2, 3$ ) was found to be  $(1.36 \pm 0.02, 0.80 \pm 0.01, 0.96 \pm 0.01)$  km s<sup>-1</sup>, their mean Solar motion ( $S_{\odot}$ ) was determined to be approximately  $18.62 \pm 4.32$  km s<sup>-1</sup>, convergent point coordinates ( $A_o$ ,  $D_o$ ) were  $(95^{\circ}.91 \pm 0^{\circ}.09, -44^{\circ}.42 \pm 0^{\circ}.02)$ , and Oort's constants, yielding  $A = 17.80 \pm 0.24$  km s<sup>-1</sup> kpc<sup>-1</sup> and  $B = -9.61 \pm 0.32$  km s<sup>-1</sup> kpc<sup>-1</sup>. Finally, the density distribution function per absolute magnitudes of USC and Oph associations is examined to obtain both luminosity and mass functions; their analysis revealed the absence of any peaks or dips as consistent with other recent studies.

**KEYWORDS:**

Upper Scorpius; Ophiuchus; velocity ellipsoid parameters; Oort's constants; luminosity function; mass function.

## 1 | INTRODUCTION

The Scorpius-Centaurus OB association (Sco-Cen) is the nearest massive star formation vicinity to the Sun, spanning a large area in the sky due to its proximity (Preibisch & Mamajek, 2008; Žerjal, Ireland, Crundall, Krumholz, & Rains, 2023). Ambartsumian (1947) coined the term “association” to describe these clusters of OB stars, highlighting that their stellar mass density often falls below  $0.1 M_{\odot} \text{pc}^{-3}$ . OB associations are relatively young as Bok (1934) demonstrated that such low-density star clusters are unstable against Galactic tidal forces (Ambartsumian, 1949). The Gaia mission's precision astrometry (Gaia Collaboration et al., 2018, 2021, 2016) has allowed for a more detailed view of the association, resulting in a rise in the number of confirmed Sco-Cen members

from just 512 stars (de Zeeuw, Hoogerwerf, de Bruijne, Brown, & Blaauw, 1999) to nearly 15,000 candidate objects (Damiani, Prisinzano, Pillitteri, Micela, & Sciortino, 2019).

Three groupings have historically been identified within Sco-Cen: Upper Scorpius (USC), Upper Centaurus-Lupus (UCL), and Lower Centaurus-Crux (LCC) (Blaauw, 1964). Numerous studies employing evolutionary models that incorporate various physical parameters indicate that the USC associations are indeed young  $\sim 5$ -10 Myr (Pecaut & Mamajek, 2016; Preibisch, Brown, Bridges, Guenther, & Zinnecker, 2002) and located at distance  $d \sim 145$  pc (Preibisch & Mamajek, 2008). The majority star formation studies, including those examining the mass function (Miret-Roig, Bouy, et al., 2022) and disc and planet formation (Barenfeld, Carpenter, Ricci, & Isella, 2016; Esplin, Luhman, Miller, & Mamajek, 2018; Richert et al., 2018), have been significantly influenced by this age uncertainty.

With a high concentration of protostars and cold gas, the Ophiuchus (Oph) molecular cloud (MC) is one of the densest areas of the Sco-Cen as part of the association. The region occupied by USC and Oph is one of the nearest star forming complexes, providing an ideal laboratory for studying the initiation and propagation of star formation through MCs (Miret-Roig, Bouy, et al., 2022). Although USC is located near the Oph star-forming clouds ( $345^\circ \leq l \leq 10^\circ$ ,  $0^\circ \leq b \leq 25^\circ$ ), no signs of active star formation are currently observed.

A comprehensive census of the USC association members requires wide-field imaging data due to its large spatial extent, covering approximately ( $\sim 100 \text{ deg}^2$ ) of the sky. Given the low extinction in USC ( $A_V < 3 \text{ mag}$ ), extensive field surveys have been conducted across a wide range of wavelengths to map the region (e.g., Lodieu, Hambly, and Jameson (2006); Slesnick, Carpenter, and Hillenbrand (2006); Rizzuto, Ireland, and Kraus (2015); Pecaut and Mamajek (2016)). The USC association includes many of the bright stars in the constellations Scorpius (Sco), Lupus, Centaurus, and Crux, including Antares, the most massive star in USC, and the majority of the stars in the Southern Cross (Preibisch & Mamajek, 2008). The MCs in Oph region have already dissipated, allowing for the observation of cluster members spanning a wide range of masses. An examination of the association’s high-mass star population ( $M \geq 2M_\odot$ ) (de Zeeuw et al., 1999) determined that the majority of the group’s members exhibit spectral types *B*, *A*, and *F*.

The study aims to re-examine and report the spatial structures, kinematics of the USC and Oph complex, including their velocity ellipsoid motion characteristics, parameters characterizing the local rotational properties of our Galaxy, such as Oort’s constants *A* and *B*, and their distribution among luminosity and mass functions.

In the context of our ongoing investigations into stellar associations, we present velocity ellipsoid parameters (VEPs) for the USC and Oph associations, derived from Gaia data. Our previous studies have explored VEPs for various associations, including those of cool and ultra-cool stars (Elsanhoury, 2016), the kinematics and ellipsoidal motion of mid-to-late M-type stars (Elsanhoury, Nouh, Branham, & Al-Johani, 2021), K dwarfs (Elsanhoury & Al-Johani, 2023), inner-halo hot sub-dwarfs (Elsanhoury, 2024), and for our first series, (Elsanhoury, Nouh, & Abdel-Rahman, 2015) its considered to compute the velocity ellipsoid of Solar neighborhood white dwarfs located  $\sim 25 \text{ pc}$ .

The remainder of this paper is structured as follows: Section 2 provides an overview of the selected data. Section 3 details the computational methods, including inner kinematics, convergent point analysis, Solar element determination, and the

Oort constants. Section 5 refers to luminosity and mass functions within USC and Oph associations. Finally, Section 6 presents the discussion and conclusions.

## 2 | DATA AND SAMPLE SELECTION

The data used in this analysis is aimed to build a census of known members within both the USC and Oph associations. The Gaia mission, originally known as the Global Astrometric Interferometer for Astrophysics, is a project by the European Space Agency designed to create the most comprehensive and accurate three-dimensional map of our Galaxy. Gaia is conducting an unprecedented survey of one percent of the Galaxy’s 100 billion stars with microarcsecond ( $\mu\text{as}$ ) precision.

The third data release (DR3) from Gaia mission (Gaia Collaboration et al., 2023) (hereafter DR3) represents a major milestone in astronomy. DR3 includes five-parameter astrometry for approximately 1.8 billion sources, providing data on sky positions ( $\alpha$ ,  $\delta$ ), parallaxes ( $\pi$ ; mas), and proper motion components in right ascension and declination ( $\mu_\alpha \cos \delta$ ,  $\mu_\delta$ ; mas yr<sup>-1</sup>), with a limiting magnitude of  $G = 21 \text{ mag}$ . The uncertainties in proper motion measurements vary: 0.02–0.03 mas yr<sup>-1</sup> for sources with  $G < 15 \text{ mag}$ , 0.07 mas yr<sup>-1</sup> for  $G \sim 17 \text{ mag}$ , 0.50 mas yr<sup>-1</sup> for  $G \sim 20 \text{ mag}$ , and 1.40 mas yr<sup>-1</sup> for  $G = 21$ . Gaia parallax errors are  $\sim 0.02\text{--}0.03 \text{ mas}$  for  $G < 15 \text{ mag}$ ,  $\sim 0.07 \text{ mas}$  for  $G = 17 \text{ mag}$ ,  $\sim 0.50 \text{ mas}$  for  $G = 20 \text{ mag}$ , and  $\sim 1.30 \text{ mas}$  for  $G = 21$ .

Radial velocities ( $V_r$ ; km s<sup>-1</sup>) for approximately 7 million stars from DR2 were also incorporated into the DR3 dataset (Gaia Collaboration et al., 2021). Notably, DR3 features improved astrometric accuracy, with a twofold improvement in proper motion accuracy and approximately a 1.5-fold improvement in parallax accuracy compared to DR2. Additionally, proper motion measurements experienced a 2.5-fold improvement, while parallax measurements experienced a 30–40% reduction in astrometric inaccuracies.

For this study, we focused on three specific Programs:

1) Program I: established by Galli, Joncour, and Moraux (2018)<sup>1</sup>, compiled a list of 1322 likely member stars of the USC association, originally derived from the Two Micron All-Sky Survey (2MASS) (Skrutskie et al., 2006). This selection was based on youth diagnostics and proper motions (Barenfeld et al., 2016; de Zeeuw et al., 1999; Luhman & Mamajek, 2012; Preibisch et al., 2002; Preibisch & Zinnecker, 1999; Rizzuto et al., 2015; Rizzuto, Ireland, & Robertson, 2011). Trigonometric parallaxes and proper motions were sourced from the Tycho–Gaia Astrometric Solution (TGAS) (Lindgren et al.,

<sup>1</sup><https://vizier.cds.unistra.fr/viz-bin/VizieR?-source=J/MNRAS/477/L50>

2016). After comparing the proper motions of stars in their sample, as provided by several catalogs, Galli et al. (2018) identified a few outliers in the fifth United States Naval Observatory CCD Astrograph Catalog (UCAC5) (Zacharias et al., 2013). Consequently, they supplemented the UCAC5 proper motions with data from the fourth Southern Proper Motion Catalog (SPM4) (Girard et al., 2011), TGAS, and the Hot Stuff for One Year catalog (Altmann, Roeser, Demleitner, Bastian, & Schilbach, 2017), which served as their primary source of proper motions. Additionally, they used data mining tools from the Strasbourg Astronomical Data Center (CDS/SIMBAD) (Wenger et al., 2000) and other sources (e.g., Kordopatis et al. (2013); Malo et al. (2014); Song, Zuckerman, and Bessell (2012); Mann et al. (2016)) to search the available literature for information on radial velocity. In total, they discovered the radial velocities of 146 stars.

For the present study, the downloaded kinematic data of ( $U$ ,  $V$ , and  $W$ ; km s<sup>-1</sup>) was done from Galli et al. (2018) to create the worksheet data required for constructing our first Program of USC, followed by updated using the most recent data from Gaia Collaboration (2022). To ensure data consistency cross-match were carried out using software that was based on the Tool for OPERations on Catalogues And Tables (TOPCAT) and Starlink Tables Infrastructure Library (STIL) (Taylor, 2005). This tool is particularly robust in analyzing tabular data within a specified range ( $0 \leq x < 1$ ) and offers numerous features for manipulating astronomical catalogs. Through this process, we identified 51 true members, as listed in Table 1. The table keys are organized as follows: the first column represents the equatorial coordinates ( $\alpha$ ,  $\delta$ )<sub>2016</sub>, the second and third columns contain 2MASS and Gaia DR3 identifier numbers, respectively, and the last three columns list the spatial velocities ( $U$ ,  $V$ , and  $W$ ; km s<sup>-1</sup>) with their uncertainties ( $\sigma_U$ ,  $\sigma_V$ , and  $\sigma_W$ ; km s<sup>-1</sup>) relative to the Galactic coordinates system.

2) Program II: was created using DR2 data (Gaia Collaboration et al., 2018) and new spectroscopy of probable members to significantly enhance the USC census within the Sco-Cen association by Luhman and Esplin (2020)<sup>2</sup>, they utilized the latest Gaia DR2 to update the most recent USC census compiled by Luhman, Herrmann, Mamajek, Esplin, and Pecaut (2018) and identified probable young stars within the Sco-Cen association (de Zeeuw et al., 1999) using a color-magnitude diagram built using Gaia DR2 data. To establish kinematic criteria for membership within that population, they focused on probable members within the USC association's center concentration. These kinematic criteria, applied to Gaia DR2,

were used to revise the list of possible USC members initially chosen by Luhman et al. (2018). They aim to finalize the analysis of candidates covering spectral types up to  $\sim L0$  ( $\sim 0.01 M_{\odot}$ ) for regions included in the United Kingdom Infrared Telescope Infrared Deep Sky Survey (UKIDSS) (Lawrence et al., 2007), which essentially includes most of USC. Based on updated data from DR3 (Gaia Collaboration et al., 2023), identified approximately 209 USC association members with different spectral types, including A- (7 points), B- (17 points), F- (24 points), G- (19 points), K- (59 points), and M-types (83 points). For kinematic analysis, the analysis focused on the last two spectral types (i.e., K and M types) comprising 142 stars, as the sample sizes for the first four types are relatively small. The data for these stars are presented in Table 2, following the same format as in Table 1.

3) Program III: Miret-Roig, Galli, et al. (2022)<sup>3</sup> identified seven different groups in the USC and Oph star forming regions. Due to the proximity of USC to the Oph star-forming clouds, no ongoing star formation is indicated. The molecular clouds in this region have already dispersed, although members of varying masses are still observable (Richert et al., 2018).

Two groups ( $\rho$  Oph and  $\alpha$  Sco) are located in Oph, four groups ( $\gamma$  Sco,  $\beta$  Sco,  $\sigma$  Sco, and  $\delta$  Sco) are in USC and share a common origin, and the seventh group ( $\pi$  Sco) represents a nearby young population. These groups exhibit an age gradient, indicating that star creation in the region has been a sequential process throughout the previous 5 Myr, ranging from the youngest Oph group to the oldest Sco group ( $\lesssim 5$  Myr). Their trace-back analysis revealed the Oph and USC groups share a common parent.

Using the Hipparcos or DR3 catalogs, the USC and Oph member stars formed the initial sample, as selected by researchers (Miret-Roig, Bouy, et al., 2022; Miret-Roig, Galli, et al., 2022). The present study identifies approximately 670 probable DR3 members from these associations, divided into seven groups: i)  $\alpha$  Sco (135 stars), ii)  $\beta$  Sco (61 stars), iii)  $\delta$  Sco (131 stars), iv)  $\sigma$  Sco (104 stars), v)  $\mu$  Sco (57 stars), vi)  $\pi$  Sco (88 stars), and vii)  $\rho$  Oph (94 stars). The data for these members are presented in Table 3, with the following format: the first column represents the equatorial coordinates ( $\alpha$ ,  $\delta$ )<sub>2016</sub>, the second column represents Gaia DR3 identifier number, and the last three columns display the spatial velocities with their uncertainty errors relative to the Galactic coordinates.

Figure 1 illustrates the distribution of radial velocities ( $V_r$ ; km s<sup>-1</sup>) as a function of Galactic longitude ( $l^{\circ}$ ) for Programs I, II, and III.

<sup>2</sup><https://vizier.cds.unistra.fr/viz-bin/VizieR?-source=J/AJ/160/44>

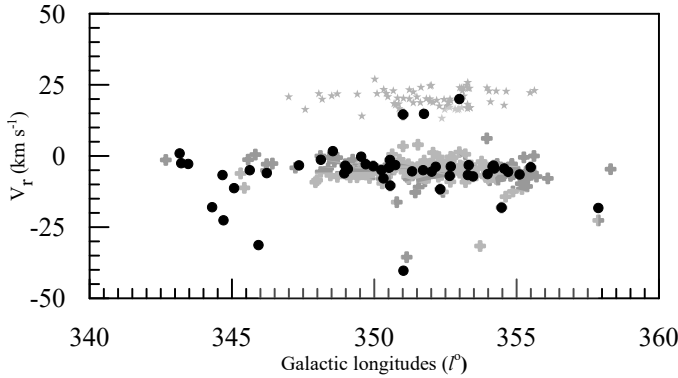
<sup>3</sup><https://vizier.cds.unistra.fr/viz-bin/VizieR?-source=J/A+A/667/A163>

**TABLE 1** Program I: Spatial velocities for 51 USC association (Galli et al., 2018)

$(\alpha, \delta)_{2016}^o$	2MASS	Gaia DR3	$U \pm \sigma_U$ km s <sup>-1</sup>	$V \pm \sigma_V$ km s <sup>-1</sup>	$W \pm \sigma_W$ km s <sup>-1</sup>
232.590, -20.613	J15302162-2036481	6253617213575749376	-30.20±0.90	-14.30±1.60	-17.80±1.40
233.817, -25.734	J15351610-2544030	6237729751586459392	-6.00±1.30	-17.90±2.20	-4.70±1.90
235.278, -26.941	J15410679-2656263	6234377340635038848	-5.70±2.30	-16.90±3.90	-5.70±3.40
...	...	...	...	...	...

**TABLE 2** Program II: Spatial velocities for 59 K-type and 83 M-type of USC association (Luhman & Esplin, 2020)

$(\alpha, \delta)_{2016}^o$	2MASS	Gaia DR3	$U \pm \sigma_U$ km s <sup>-1</sup>	$V \pm \sigma_V$ km s <sup>-1</sup>	$W \pm \sigma_W$ km s <sup>-1</sup>
K-type; 59 points					
240.898, -22.766	J16033550-2245560	6243154501445899264	-10.28 ± 0.17	-15.52 ± 0.24	-9.04 ± 0.12
243.327, -22.214	J16131858-2212489	6242687277719794176	-6.37 ± 0.37	-14.77 ± 0.23	-8.10 ± 0.18
244.381, -23.060	J16173138-2303360	6050373760491905920	-3.92 ± 0.38	-14.66 ± 0.11	-5.41 ± 0.15
...	...	...	...	...	...
M-type; 83 points					
236.522, -29.348	J15460529-2920531	6233037070321568128	-3.44 ± 3.14	-16.61 ± 0.99	-8.75 ± 1.18
239.579, -20.907	J15581906-2054238	6246706714275425024	-5.88 ± 1.05	-16.03 ± 0.21	-6.58 ± 0.48
241.381, -19.762	J16053153-1945435	6247208950571840640	3.83 ± 1.64	-14.11 ± 0.27	-6.36 ± 0.73
...	...	...	...	...	...

**FIGURE 1** Distribution of radial velocities ( $V_r$ ; km s<sup>-1</sup>) of USC and Oph member association stars versus their Galactic longitudes ( $l^\circ$ ) for the three Programs. Data points are represented as black closed circles (Program I), middle gray closed pluses (Program II), and faint gray closed stars (Program III).

### 3 | COMPUTATIONAL METHODS

#### 3.1 | Inner kinematics and VEPs

Let  $d$ (pc) be the distance from the Sun to the star, and, because the observation data for proper motions are always given in the

equatorial system, let us resolve positions and velocities into equatorial rectangular components (Smart, 1968),

$$\begin{aligned} x &= d \cos \delta \cos \alpha, \\ y &= d \cos \delta \sin \alpha, \\ z &= d \sin \delta. \end{aligned} \quad (1)$$

Differentiation Eqs. (1) with respect to time, we have the equatorial components of the stellar velocity with respect to the Sun.

$$\begin{aligned} V_x &= \dot{d} \cos \delta \cos \alpha - \dot{\alpha} d \cos \delta \sin \alpha - \dot{\delta} d \sin \delta \cos \alpha, \\ V_y &= \dot{d} \cos \delta \sin \alpha + \dot{\alpha} d \cos \delta \cos \alpha - \dot{\delta} d \sin \delta \sin \alpha, \\ V_z &= \dot{d} \sin \delta + \dot{\delta} d \cos \delta. \end{aligned} \quad (2)$$

The quantity  $\dot{d}$  stands for the radial velocity ( $V_r$ ; km s<sup>-1</sup>) and  $\dot{\alpha} d \cos \delta$  and  $\dot{\delta} d$  are traverse velocities (i.e.,  $\dot{\alpha} d \cos \delta = V_\alpha = 4.74 d \mu_\alpha \cos \delta$  and  $\dot{\delta} d = V_\delta = 4.74 d \mu_\delta$ ; km s<sup>-1</sup>) and may be written as

$$\begin{bmatrix} V_x \\ V_y \\ V_z \end{bmatrix} = \begin{bmatrix} V_r \\ V_\alpha \\ V_\delta \end{bmatrix} \cdot \begin{bmatrix} \cos \alpha \cos \delta & -\sin \alpha & -\cos \alpha \sin \delta \\ \sin \alpha \cos \delta & \cos \alpha & -\sin \alpha \sin \delta \\ \sin \delta & 0 & \cos \delta \end{bmatrix} \quad (3)$$

**TABLE 3** Program III: 670 members of USC and Oph associations for seven identified groups (Miret-Roig, Galli, et al., 2022)

$(\alpha, \delta)_{2016}^o$	Gaia DR3	$U \pm \sigma_U$ km s <sup>-1</sup>	$V \pm \sigma_V$ km s <sup>-1</sup>	$W \pm \sigma_W$ km s <sup>-1</sup>
$\alpha$ Sco; 135 stars				
244.872, -21.404	6244295760151546624	-2.68 ± 0.45	-16.71 ± 0.07	-5.86 ± 0.17
243.633, -28.123	6042179203410212864	-3.43 ± 0.10	-16.29 ± 0.07	-5.52 ± 0.05
246.460, -28.344	6044217320011144832	-2.86 ± 0.10	-16.12 ± 0.13	-5.472 ± 0.07
...	...	...	...	...
$\beta$ Sco; 61 stars				
241.610, -23.103	6242336396077230720	-2.68 ± 0.21	-16.98 ± 0.20	-6.88 ± 0.12
241.705, -22.277	6242541558069369216	-0.83 ± 0.39	-16.76 ± 0.39	-7.29 ± 0.26
243.556, -22.750	6242595262340274688	0.19 ± 0.15	-17.01 ± 0.12	-7.00 ± 0.08
...	...	...	...	...
$\delta$ Sco; 131 stars				
240.845, -25.755	6043652720795418496	-5.89 ± 0.09	-16.79 ± 0.06	-7.44 ± 0.04
244.227, -25.431	6048832623143380480	-6.21 ± 0.25	-16.08 ± 0.24	-10.07 ± 0.16
243.725, -25.075	6049525830867571072	-7.00 ± 0.12	-15.89 ± 0.11	-9.51 ± 0.07
...	...	...	...	...
$\sigma$ Sco; 104 stars				
238.341, -21.971	6240546906538196352	-4.94 ± 0.21	-16.32 ± 0.09	-7.90 ± 0.10
244.105, -24.989	6049614307192716288	-7.74 ± 0.56	-16.96 ± 0.12	-6.35 ± 0.19
245.846, -29.026	6038188148001109248	-6.04 ± 0.23	-14.73 ± 0.19	-6.03 ± 0.10
...	...	...	...	...
$\mu$ Sco; 57 stars				
242.261, -18.996	6248783275121192704	-6.79 ± 0.88	-14.16 ± 0.10	-9.92 ± 0.39
243.091, -19.579	6245692620954228864	-9.04 ± 0.52	-14.81 ± 0.08	-9.66 ± 0.22
243.095, -21.455	6243054686400695040	-5.10 ± 0.25	-15.79 ± 0.22	-9.43 ± 0.16
...	...	...	...	...
$\pi$ Sco; 88 stars				
236.847, -25.868	6234897925031130624	-8.90 ± 0.49	-17.53 ± 0.15	-5.63 ± 0.21
242.541, -24.583	6049847575458556800	-4.72 ± 0.89	-18.96 ± 0.17	-5.53 ± 0.32
243.025, -23.246	6242180368499938816	-8.39 ± 0.62	-16.75 ± 0.10	-4.54 ± 0.23
...	...	...	...	...
$\rho$ Oph; 94 stars				
245.209, -22.594	6050496459111584384	-8.65 ± 0.33	-13.88 ± 0.06	-6.38 ± 0.12
246.386, -26.194	6045872806564888192	-5.12 ± 0.20	-14.68 ± 0.10	-9.15 ± 0.08
247.266, -24.862	6046072986395944064	-7.59 ± 0.20	-15.37 ± 0.18	-8.75 ± 0.12
...	...	...	...	...

To facilitate the analysis, we must solve Eqs. (2) for  $V_r$ ,  $V_\alpha$ , and  $V_\delta$ , so that we can write equations that involve only radial velocities or only proper motions.

$$\begin{aligned}
 V_x \cos \delta \cos \alpha + V_y \cos \delta \sin \alpha + V_z \sin \delta &= V_r, \\
 -V_x \sin \delta \cos \alpha - V_y \sin \delta \sin \alpha + V_z \cos \delta &= 4.74d\mu_\delta, \\
 -V_x \sin \alpha + V_y \cos \alpha &= 4.74d\mu_\alpha \cos \delta.
 \end{aligned}
 \tag{4}$$

The transformation of equatorial velocities in Eqs. (2) to Galactic velocities ( $U$ ,  $V$ ,  $W$ ; km s<sup>-1</sup>), being determined by the definition of the equatorial positions of the North Galactic Pole and zero Galactic longitude, therefore, according to Johnson and Soderblom (1987).

$$\begin{bmatrix} U \\ V \\ W \end{bmatrix} = B \cdot \begin{bmatrix} V_r \\ V_\alpha \\ V_\delta \end{bmatrix} \quad (5)$$

where  $B = T \cdot A$ ,

$$T = \begin{bmatrix} -0.06699 & -0.87276 & -0.48354 \\ +0.49273 & -0.45035 & +0.74458 \\ -0.86760 & -0.18837 & +0.46020 \end{bmatrix}$$

and

$$A \equiv \begin{bmatrix} +\cos \alpha \cos \delta & -\sin \alpha & -\cos \alpha \sin \delta \\ +\sin \alpha \cos \delta & +\cos \alpha & -\sin \alpha \sin \delta \\ +\sin \delta & 0 & +\cos \delta \end{bmatrix}$$

The solution is easy to write because the matrix of coefficients in Eqs. (5) is orthogonal, so that its inverse equals its transpose. We find that

$$\begin{aligned} U &= -0.06699 V_x - 0.87276 V_y - 0.48354 V_z, \\ V &= +0.49273 V_x - 0.45035 V_y + 0.74458 V_z, \\ W &= -0.86760 V_x - 0.18837 V_y + 0.46020 V_z. \end{aligned} \quad (6)$$

On the other hand, the derivations are well defined considering Eqs. (2) by using an equatorial-Galactic transformation matrix based on the SPECFIND v2.0 catalog of radio continuum spectra; see Eq. (14) in Liu, Zhu, and Hu (2011) (printed to 10 decimals, 1 mas accuracy):

$$\begin{aligned} U &= -0.0518807421 V_x - 0.8722226427 V_y \\ &\quad - 0.4863497200 V_z, \\ V &= +0.4846922369 V_x - 0.4477920852 V_y \\ &\quad + 0.7513692061 V_z, \\ W &= -0.8731447899 V_x - 0.1967483417 V_y \\ &\quad + 0.4459913295 V_z, \end{aligned} \quad (7)$$

To specify VEPs as outlined in the literature (Elsanhoury, 2024; Elsanhoury & Al-Johani, 2023), considering estimation of the velocities dispersion ( $\sigma_1$ ,  $\sigma_2$  and  $\sigma_3$ ; km s<sup>-1</sup>) using the following expressions:

$$\begin{aligned} \sigma_1 &= \sqrt{2\rho^{\frac{1}{3}} \cos \frac{\phi}{3} - \frac{k_1}{3}}, \\ \sigma_2 &= \sqrt{-\rho^{\frac{1}{3}} \left\{ \cos \frac{\phi}{3} + \sqrt{3} \sin \frac{\phi}{3} \right\} - \frac{k_1}{3}}, \\ \sigma_3 &= \sqrt{-\rho^{\frac{1}{3}} \left\{ \cos \frac{\phi}{3} - \sqrt{3} \sin \frac{\phi}{3} \right\} - \frac{k_1}{3}}. \end{aligned} \quad (8)$$

The parameters  $q$  and  $r$  are given by the equations:

$$q = \frac{1}{3}k_2 - \frac{1}{9}k_1^2 \quad ; \quad r = \frac{1}{6}(k_1k_2 - 3k_3) - \frac{1}{27}k_1^3 \quad (9)$$

$\rho$  and  $\phi$  are calculated as:

$$\rho = \sqrt{-q^3}, \quad (10)$$

$$x = \rho^2 - r^2, \quad (11)$$

$$\phi = \tan^{-1} \left( \frac{\sqrt{x}}{r} \right). \quad (12)$$

The coefficients  $k_1$ ,  $k_2$ , and  $k_3$  are determined as:

$$\begin{aligned} k_1 &= -(\mu_{11} + \mu_{22} + \mu_{33}), \\ k_2 &= \mu_{11}\mu_{22} + \mu_{11}\mu_{33} + \mu_{22}\mu_{33} - (\mu_{12}^2 + \mu_{13}^2 + \mu_{23}^2), \\ k_3 &= \mu_{12}^2\mu_{33} + \mu_{13}^2\mu_{22} + \mu_{23}^2\mu_{11} - \mu_{11}\mu_{22}\mu_{33} - 2\mu_{12}\mu_{13}\mu_{23}. \end{aligned} \quad (13)$$

and the matrix elements ( $\mu_{ij}$ ) are

$$\begin{aligned} \mu_{11} &= \frac{1}{N} \sum_{i=1}^N U_i^2 - (\bar{U})^2; \quad \mu_{12} = \frac{1}{N} \sum_{i=1}^N U_i V_i - \bar{U} \bar{V}; \\ \mu_{13} &= \frac{1}{N} \sum_{i=1}^N U_i W_i - \bar{U} \bar{W}; \quad \mu_{22} = \frac{1}{N} \sum_{i=1}^N V_i^2 - (\bar{V})^2; \\ \mu_{23} &= \frac{1}{N} \sum_{i=1}^N V_i W_i - \bar{V} \bar{W}; \quad \mu_{33} = \frac{1}{N} \sum_{i=1}^N W_i^2 - (\bar{W})^2. \end{aligned} \quad (14)$$

Accordingly, Figure 2 presents the distribution of the Galactic spatial velocities components ( $U$ ,  $V$ ,  $W$ ) for our retrieved three Programs with their figures keys.

## 3.2 | CP

Nearby star associations that share a common space motion exhibit proper motions that seem to "converge" towards one specific sky point and share similarities within the Galaxy as they are gravitationally bound. Therefore, the parameters such as age, distance, chemical composition, and kinematics (internal motion or trajectory) are correlated. The converge can be understood as accumulations of stars moving with a common velocity vector, their parallel motions on the celestial sphere will direct them toward a coherent point, known as the vertex, apex, or convergent point (CP) of the open clusters (OCs) and/or associations. Computing the apex position assumes that the moving group is neither expanding, contracting, nor rotating, and that its motion relative to the field is significant enough to enable accurate membership discrimination. Vereshchagin, Chupina, Sariya, Yadav, and Kumar (2014), Elsanhoury et al. (2018), Bisht et al. (2020), Elsanhoury (2021), and Maurya, Joshi, Elsanhoury, and Sharma (2021) used the method of individual star apex (AD-diagram) as described by Chupina, Reva, and Vereshchagin (2001, 2006). This method utilizes average space velocity vectors, as expressed in Eqs. (2), to determine the equatorial coordinates of the CP ( $A_o$ ,  $D_o$ ) in the following forms:

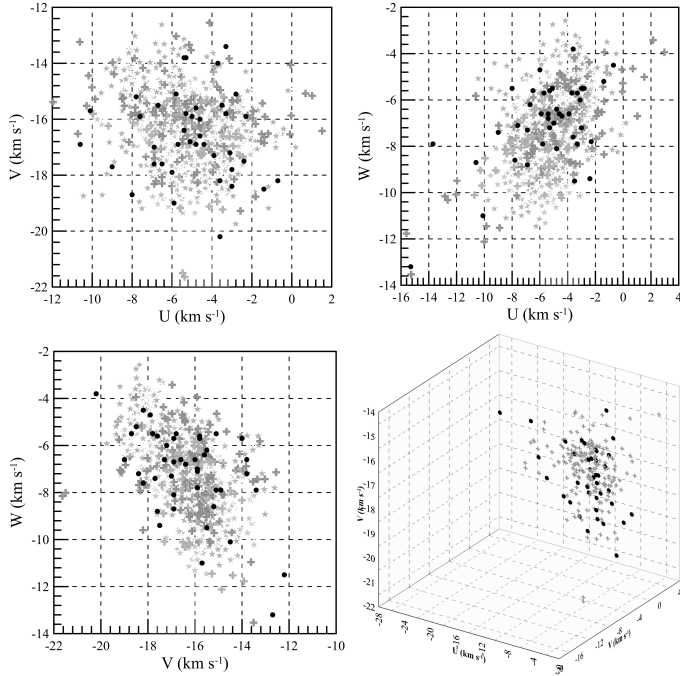


**FIGURE 2** Distribution of spatial velocity components: ( $V$  vs.  $U$ ), ( $W$  vs.  $U$ ), and ( $W$  vs.  $V$ ) along the Galactic coordinates for three Programs. Data points are represented as black closed circles (Program I), middle gray closed pluses (Program II), and faint gray closed stars (Program III). The figure also displays their 3D array representation.

$$\begin{aligned} A_o &= \tan^{-1} \left( \frac{\overline{V}_y}{\overline{V}_x} \right) \\ D_o &= \tan^{-1} \left( \frac{\overline{V}_z}{\sqrt{\overline{V}_x^2 + \overline{V}_y^2}} \right) \end{aligned} \quad (15)$$

The cross mark in Figure 3 shows the apex position of Program III as listed in Table 4 .

### 3.3 | Solar motion elements

Consider a group with mean spatial velocities ( $\overline{U}$ ,  $\overline{V}$ ,  $\overline{W}$ ) along the Galactic coordinates, based on observational data. The components of the Sun's velocities ( $U_\odot$ ,  $V_\odot$  and  $W_\odot$ ) are expressed as follows:  $U_\odot = -\overline{U} = -S_\odot \cos l_A \cos b_A$ ,  $V_\odot = -\overline{V} = S_\odot \cos l_A \sin b_A$ , and  $W_\odot = -\overline{W} = S_\odot \sin b_A$ . As a result, we determine the Solar elements, i.e.,

$$S_\odot = \sqrt{\overline{U}^2 + \overline{V}^2 + \overline{W}^2}, \quad (16)$$

$$l_A = \tan^{-1} \left( \frac{-\overline{V}}{\overline{U}} \right), \quad (17)$$

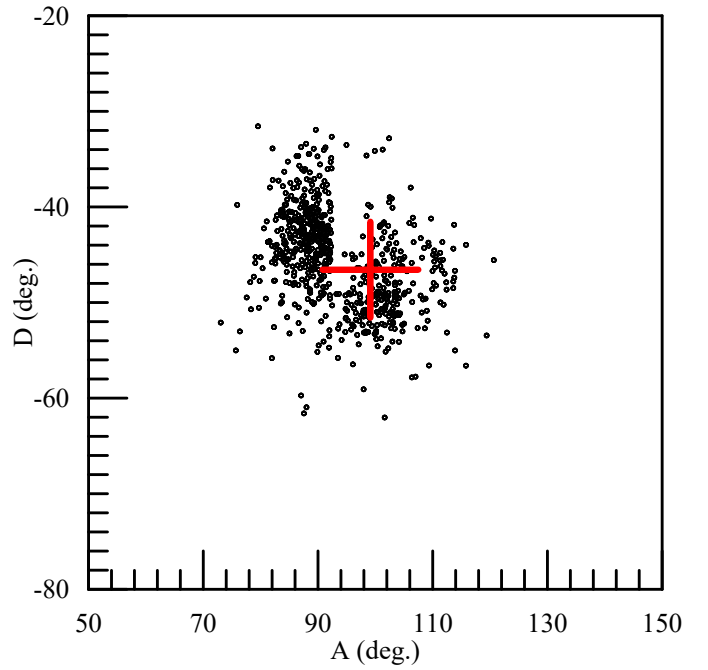


**FIGURE 3** AD-diagram of Program III associations, showing 670 points with the cross point ( $A_o$ ,  $D_o$ ) indicated.

$$b_A = \sin^{-1} \left( \frac{-\overline{W}}{S_\odot} \right). \quad (18)$$

The Sun's velocities were relative to these groups and the same axes are defined as ( $X_\odot^\bullet = -\overline{V}_x$ ), ( $Y_\odot^\bullet = -\overline{V}_y$ ), and ( $Z_\odot^\bullet = -\overline{V}_z$ ), taking into account the position along the  $x$ ,  $y$ , and  $z$  - axes in the coordinate system centered around the Sun (i.e., equatorial coordinates). Consequently, we are obtained with Solar components that have radial velocities.

$$S_\odot = \sqrt{(X_\odot^\bullet)^2 + (Y_\odot^\bullet)^2 + (Z_\odot^\bullet)^2}, \quad (19)$$

$$\alpha_A = \tan^{-1} \left( \frac{Y_\odot^\bullet}{X_\odot^\bullet} \right), \quad (20)$$

$$\delta_A = \tan^{-1} \left( \frac{Z_\odot^\bullet}{\sqrt{(X_\odot^\bullet)^2 + (Y_\odot^\bullet)^2}} \right). \quad (21)$$

### 3.4 | Rotational A & B constants

Many kinematic and photometric parameters can be extracted from OCs and/or stellar associations with great accuracy. These parameters are essential for studying the Galaxy and its subsystems. Nearby stellar associations serve as valuable tools for investigating the characteristics of the thick and thin disks of the Galaxy, including their chemical and dynamical history, spiral structure, star formation, and distance scale determination.

**TABLE 4** The kinematics, VEPs, Solar elements, and the convergent points retrieved for Programs I, II, and III.

Program	$N$	$(\bar{V}_x, \bar{V}_y, \bar{V}_z; \text{km s}^{-1})$	$(\bar{U}, \bar{V}, \bar{W}; \text{km s}^{-1})$	$(\sigma_1, \sigma_2, \sigma_3; \text{km s}^{-1})$	$(S_G; \text{km s}^{-1})$	$(U_A, b_A)^\rho$	$(e_A, \delta_A)^\rho$	$(A_0, D_0)^\rho$
I	51	-1.10E+003, 1.49E+3.87, -11.90E+3.45	-7.21E+2.69, -16.17E+4.02, -7.29E+2.70	19.69E+4.43, 10.41E+3.23, 1.63E+0.78	19.14E+4.37	-65.97E+2.38	-85.80, 38.43	94.21E+0.11, -38.43E+0.02
II: K-type	59	-1.18E+003, 1.27E+3.57, -12.77E+3.57	-4.82E+0.46, -15.85E+3.98, -7.17E+2.68	17.95E+4.23, 2.61E+0.62, 1.14E+0.94	18.06E+4.25	-73.10, 23.40	-84.70, 45.00	95.30E+0.10, -50.00E+0.01
II: M-type	83	-0.81E+003, 1.36E+3.70, -12.76E+3.57	-5.67E+0.42, -16.10E+4.01, -7.67E+2.77	18.64E+4.32, 2.56E+0.63, 1.19E+0.09	18.71E+4.33	-70.61, 24.21	-86.61, 43.00	95.40E+0.10, -43.00E+0.02
III: $\alpha$ Sco	135	-2.78E+060, 1.168E+3.42, -13.38E+3.66	-3.54E+0.53, -16.63E+4.08, -5.85E+0.41	1.00E+0.00, 0.70E+0.01, 0.60E+0.01	18.00E+4.24	-78.00, 18.98	-76.62, 48.10	103.39E+0.09, -48.10E+0.01
III: $\beta$ Sco	61	-1.54E+003, 1.49E+3.57, -13.71E+3.70	-3.17E+0.56, -16.13E+4.02, -7.00E+2.65	1.10E+0.01, 0.30E+0.00, 0.70E+0.01	17.87E+4.23	-78.90, 23.07	-82.28, 50.10	97.72E+0.10, -50.10E+0.01
III: $\delta$ Sco	131	-0.80E+003, 1.42E+3.77, -12.58E+3.55	-6.26E+2.50, -16.22E+4.03, -7.72E+2.78	0.80E+0.01, 0.60E+0.01, 0.75E+0.01	19.02E+4.36	-68.88, 23.94	-86.79, 41.40	93.21E+0.10, -43.05E+0.02
III: $\mu$ Sco	104	-1.12E+003, 1.38E+3.72, -12.95E+3.60	-5.69E+2.38, -16.46E+4.06, -7.52E+2.74	2.20E+0.01, 1.50E+0.01, 1.10E+0.01	18.97E+4.36	-70.92, 23.35	-88.37, 43.05	94.64E+0.10, -43.05E+0.02
III: $\sigma$ Sco	57	0.44E+001, 1.371E+3.70, -12.53E+3.54	-5.88E+2.42, -15.34E+3.92, -8.67E+2.94	1.00E+0.01, 0.30E+0.01, 1.00E+0.01	18.58E+4.31	-69.01, 27.82	-88.17E+0.11, -42.41E+0.02	88.17E+0.11, -42.41E+0.02
III: $\pi$ Sco	88	-4.42E+048, 1.32E+3.64, -13.32E+3.65	-4.83E+0.45, -18.08E+4.25, -4.69E+0.46	1.80E+0.01, 0.90E+0.01, 1.00E+0.01	19.39E+4.40	-75.00, 14.08	-71.55, 43.64	108.45E+0.01, -43.64E+0.02
III: $\rho$ Sco	94	1.01E+001, 1.374E+3.71, -12.51E+3.54	-5.96E+0.41, -15.06E+3.88, -9.16E+3.03	1.60E+0.01, 0.90E+0.01, 1.20E+0.02	18.61E+4.32	-68.43, 29.50	-83.80, 42.24	83.80E+0.11, -42.24E+0.01

Based primarily on the analysis of spatial positions, the morphology of the stellar components of the Galaxy has been refined. By examining the velocities of stars, particularly those near the Sun with well-determined coordinates and velocities, one can establish a relationship between the morphological parameters of these stellar groups and the kinematic properties of the stellar population of the Galaxy.

Traditionally, the study of the stellar structure of the Galaxy has relied on the position of stars in the three spatial coordinates  $x$ ,  $y$ , and  $z$  (Tutukov, Chupina, & Vereshchagin, 2023). The components of the stellar spatial velocities ( $U$ ,  $V$ , and  $W$ ) can be determined using radial velocity spectral data, long-term observations of stellar motion in the celestial sphere with known parallaxes, and consideration of the Sun's motion within the Galaxy. DR3 catalog (Gaia Collaboration et al., 2023) which provides data for approximately two billion stars in the Galaxy is particularly effective in predicting these values.

For nearly a century, the kinematics of nearby stars have been utilized to investigate the characteristics of the Galactic disk. Oort demonstrated that the constants of the stream velocity field equation could describe the local frequency and the circular velocity gradient (Oort, 1927a, 1927b). He used radial velocities and proper motions to determine the Oort rotational constants ( $A$  &  $B$ ;  $\text{km s}^{-1} \text{ kpc}^{-1}$ ), arriving at values of  $A \approx 19 \text{ km s}^{-1} \text{ kpc}^{-1}$  and  $B \approx -24 \text{ km s}^{-1} \text{ kpc}^{-1}$ . This study refuted the notion of solid-body rotation for the Galaxy, revealing a nearly flat rotation curve. Computation of several parameters is achieved, including ratios ( $\sigma_2/\sigma_1$ ) of Programs I, II, III, and Oort's constants.

i.e.

$$\left(\frac{\sigma_2}{\sigma_1}\right)^2 = \frac{-B}{A-B}, \quad (22)$$

or

$$\frac{-B}{A} = \frac{1}{(\sigma_1/\sigma_2)^2 - 1}. \quad (23)$$

## 4 | KINEMATIC AND ROTATION RESULTS

Following the above computational scheme, a Mathematica routine was created and developed to compute the kinematics and VEPs of Programs I, II, and III in addition to Oort's constants.

Table 4 lists our original numerical results for three Programs, including various kinematic parameters of space velocities ( $\bar{V}_x$ ,  $\bar{V}_y$ ,  $\bar{V}_z$ ) and their corresponding spatial velocities  $\bar{U} = \frac{1}{N} \sum_{i=1}^N U_i$ ,  $\bar{V} = \frac{1}{N} \sum_{i=1}^N V_i$ , and  $\bar{W} = \frac{1}{N} \sum_{i=1}^N W_i$



along equatorial and Galactic coordinates, respectively, velocities dispersions ( $\sigma_1, \sigma_2, \sigma_3$ ;  $\text{km s}^{-1}$ ), Solar elements ( $S_\odot, l_A^o, b_A^o, \alpha_A^o, \delta_A^o$ ), CP coordinates ( $A_o, D_o$ ) $^o$ , and Oort's constants.

Mean spatial velocities ( $\bar{U}$ ,  $\bar{V}$ , and  $\bar{W}$ ) were calculated, and their combined value is as follows:  $V_{space} = (\bar{U}^2 + \bar{V}^2 + \bar{W}^2)^{1/2}$  ( $\text{km s}^{-1}$ ) for USC Program I ( $-7.21 \pm 2.69, -16.17 \pm 4.02, -7.29 \pm 2.70$ , and  $19.15 \pm 4.38 \text{ km s}^{-1}$ ), Program II ( $-5.25 \pm 2.29, -15.98 \pm 4.00, -7.42 \pm 2.72$ , and  $18.38 \pm 4.29 \text{ km s}^{-1}$ ), and Program III are all associated with USC and Oph (i.e.,  $-5.05 \pm 2.25, -16.27 \pm 4.03, -7.23 \pm 2.69$ , and  $18.51 \pm 4.30 \text{ km s}^{-1}$ ). These values coincide with those calculated by Galli et al. (2018) wherein ( $\bar{U} = -5.00 \pm 0.10, \bar{V} = -16.60 \pm 0.10, \bar{W} = -6.80 \pm 0.10$ , and  $18.80 \pm 0.10 \text{ km s}^{-1}$ ), according to Miret-Roig, Galli, et al. (2022) ( $-4.97, -16.27, -7.21$ ) and their  $V_{space}$  is  $18.48 \text{ km s}^{-1}$ , for 209 stars that were accepted as members of USC (Luhman & Esplin, 2020), the mean spatial velocities are ( $\bar{U}, \bar{V}, \bar{W}$ ) =  $(-5.10 \pm 4.10, -16.00 \pm 1.40, -7.20 \pm 2.10)$ , and  $\bar{U} = -6.16^{+0.14}_{-0.13}, \bar{V} = -16.89^{+0.08}_{-0.10}, \bar{W} = -7.05^{+0.09}_{-0.08} \text{ km s}^{-1}$  within DR1 for a smaller sample of members by Wright and Mamajek (2018).

Mean velocity dispersion ( $\sigma_j$ ;  $\forall j = 1, 2, 3$ ;  $\text{km s}^{-1}$ ) where ( $\sigma_1 > \sigma_2 > \sigma_3$ ). Therefore,  $\bar{\sigma}_1, \bar{\sigma}_2$ , and  $\bar{\sigma}_3$  for the three programs are as follows: Program I ( $19.60 \pm 4.43, 10.41 \pm 3.23, 1.63 \pm 0.78$ ), Program II ( $18.30 \pm 4.23, 2.60 \pm 0.62, 1.17 \pm 0.93$ ), and Program III ( $1.36 \pm 0.02, 0.80 \pm 0.01, 0.96 \pm 0.01$ ),  $\sigma$ 's are around  $1.63^{+0.20}_{-0.20}, 1.14^{+0.13}_{-0.14}$ , and  $2.51^{+0.11}_{-0.09}$  according to data achieved through DR1 (Wright & Mamajek, 2018).

The absolute value of the Sun's velocity is denoted as ( $S_\odot$ ;  $\text{km s}^{-1}$ ) considering the retrieved associations under study, where the Solar apex's Galactic longitude and latitude relative to Galactic center is ( $l_A, b_A$ ) and in the equatorial coordinates ( $\alpha_A, \delta_A$ ). The position of the apex ( $l_A, b_A$ ) in the Galactic coordinates can be calculated using basic spherical trigonometry formulas via ( $\alpha_A, \delta_A$ ). Numerically, mean absolute value of the Sun's velocity  $\bar{S}_\odot$  relative to our three program associations are  $19.14 \pm 4.37$  (Program I),  $18.39 \pm 4.29$  (Program II), and  $18.62 \pm 4.32$  (Program III). Columns seven and eight of Table 4 present estimated ( $l_A, b_A$ ) and ( $\alpha_A, \delta_A$ ), respectively.

The last column of Table 4 indicate the CP coordinates ( $A_o, D_o$ ) $^o$ ;  $94^\circ.21 \pm 0^\circ.11, -38^\circ.43 \pm 0^\circ.02$  (Program I),  $94^\circ.35 \pm 0^\circ.11, -46^\circ.50 \pm 0^\circ.15$  (Program II), and  $95^\circ.91 \pm 0^\circ.10, -44^\circ.42 \pm 0^\circ.15$  (Program III), all of which are in line with the findings of earlier research by de Bruijne (1999) into which ( $A_o = 95^\circ.20 \pm 2^\circ.20, D_o = -42^\circ.80 \pm 2^\circ.50$ ),  $A_o = 110^\circ.97 \pm 2^\circ.20$  and  $D_o = -20^\circ.25 \pm 2^\circ.50$  by Galli et al. (2018), and utilizing Jones method (Jones, 1971) Wright and Mamajek (2018) estimated CPs for USC associations as  $A_o = 116^\circ.22^{+10.70}_{-9.46}$  and  $D_o = -55^\circ.29^{+5.37}_{-4.56}$ .

The absolute value of  $A$  and  $B$  (i.e.,  $|A - B|$ ) is defined as the angular rotation rate and therefore the differential Galactic rotation rate with radius  $R_o = 8.20 \pm 0.10 \text{ pc}$  (Bland-Hawthorn

**TABLE 5** Ratios of velocities dispersion and Oort's constants devoted with three Programs and recent ones.

Program	( $\sigma_2/\sigma_1$ )	$A$ ; $\text{km s}^{-1} \text{ kpc}^{-1}$	$B$ ; $\text{km s}^{-1} \text{ kpc}^{-1}$	References
I	0.53	$8.74 \pm 0.23$	$-7.33 \pm 0.20$	Present study
II; K-type	0.15	$25.92 \pm 0.20$	$-0.15 \pm 0.01$	Present study
II; M-type	0.14	$25.93 \pm 0.20$	$-0.14 \pm 0.01$	Present study
III; $\alpha$ Sco	0.70	$13.29 \pm 0.27$	$-12.78 \pm 0.27$	Present study
III; $\beta$ Sco	0.50	$19.55 \pm 0.23$	$-6.52 \pm 0.39$	Present study
III; $\delta$ Sco	0.75	$11.41 \pm 0.30$	$-14.66 \pm 0.26$	Present study
III; $\sigma$ Sco	0.68	$14.01 \pm 0.27$	$-12.06 \pm 0.28$	Present study
III; $\mu$ Sco	0.50	$19.55 \pm 0.23$	$-6.52 \pm 0.39$	Present study
III; $\pi$ Sco	0.50	$19.55 \pm 0.23$	$-6.52 \pm 0.39$	Present study
III; $\rho$ Oph	0.56	$17.89 \pm 0.24$	$-8.18 \pm 0.35$	Present study
inner-halo hot sd	0.80	$9.38 \pm 0.34$	$-16.69 \pm 0.25$	Elsanhoury (2024)
d	0.74	$16.06 \pm 0.68$	$-19.43 \pm 1.37$	Elsanhoury et al. (2021)
K-dwarfs	-	$16.31 \pm 0.61$	$-11.99 \pm 0.79$	Wang et al. (2021)
M-dwarfs	0.71	$15.60 \pm 0.03$	$-13.90 \pm 1.80$	Nouh and Elsanhoury (2020)
-	-	$15.730 \pm 0.320$	$-12.670 \pm 0.340$	Krisanova, Bobylev, and Bajkova (2020)
-	0.83	$9.41 \pm 0.92$	$-14.24 \pm 1.38$	Bobylev and Bajkova (2019)
$d \approx 200 \text{ kpc}$	0.64	$15.21 \pm 0.58$	$-13.83 \pm 0.89$	Bobylev, Bajkova, and Gromov (2017)

et al., 2019) was provided by Oort (1927a, 1927b) at  $247.50 \text{ km s}^{-1}$  and mathematically is  $V_o = \omega_o R_o = |A - B| R_o$ . Mihalas and Binney (1981) states that  $V_o$  yields in the range of 200-300  $\text{km s}^{-1}$  based on radial velocities of globular clusters or spheroidal component stars in our Galaxy or external galaxies in the Local Group. Recently,  $V_o$  takes the values  $213.81 \pm 14.61, 204.00$ , and  $256.64 \pm 0.37 \text{ km s}^{-1}$  (Elsanhoury & Al-Johani, 2023; Li, Zhao, & Yang, 2019; Nouh & Elsanhoury, 2020) with respective manner.

According to Eq. (22) the adopted values of dispersions  $\sigma_1, \sigma_2$ , and their ratios ( $\sigma_2/\sigma_1$ ) are listed in Table 5. Considering large volume sample (i.e., Program III) into which  $\sigma_2/\sigma_1 \approx 0.60$  and its presents a good agreement when compared with recent ones and taken into account the computed value of angular rotation rate  $|A - B| \approx 26.07 \pm 5.10 \text{ km s}^{-1}$  (Elsanhoury & Al-Johani, 2023), therefore, the adopted mean values of the Oort constant are about  $A = 17.80 \pm 0.24 \text{ km s}^{-1} \text{ kpc}^{-1}$  and  $B = -9.61 \pm 0.32 \text{ km s}^{-1} \text{ kpc}^{-1}$ , these values are approximately over 80% consistency with others.

Since OB associations include many bright stars (Pecaut & Mamajek, 2016) and high-massive ones (de Zeeuw et al., 1999) those leads us to reflect and conclude that the similarities and/or differences exit between the retrieved kinematic and rotational characteristics of Programs I, II, and III are due to volume and restrictions of gathered data as mentioned above.

## 5 | LUMINOSITY AND MASS FUNCTIONS OF USC AND OPH ASSOCIATIONS

The luminosity function (LF) which is the number of stars at apparent magnitude per unit magnitude interval per unit area, allows investigators to statistically characterize the distribution of stars in the sky. All methods for determining the LF of field stars, count the number of stars as a function of their magnitudes, and several methodologies are used to estimate distances to these stars. Therefore, the absolute magnitudes and space

densities could be used to estimate the LF (McCuskey, 1966; Trumpler & Weaver, 1953; van Rhijn, 1936).

The initial mass function (IMF;  $\xi(\log \mathfrak{M})$ ) represents the outcome of the star formation history and age, and all are coded in the LF profile (Bessell & Stringfellow, 1993; Luyten, 1968).

In the present study, the classical approach of van Rhijn (1936) is used to determine LF ( $\phi(M_G)$ ),

$$\phi(M_G) = \frac{dN}{dM_G}. \quad (24)$$

This method claimed that the density of the stars is the number  $dN$  of stars per cubic parsec in the magnitude interval  $M_G$  to  $M_G + dM_G$ , and is determined by splitting the zone into shells with a specific width. A double frequency table (DFT) was created that estimates how many stars in each shell correlate to each magnitude interval per cubic parsec. Following this classical scheme of 670 USC and Oph candidates listed in Table 3 within absolute magnitudes and distances ranging from -3.510 to 9.142 mag and 86.755 to 172.387 pc, respectively, taking into account Gaia DR does not achieve completeness at the bright end of LF ( $M_G < 8$ ) (Guo, de Koter, Kaper, Brown, & de Bruijne, 2021). Therefore, DFT results are displayed here in Table 6, where the number of members is divided into equal absolute magnitude and distance intervals. The computed LF via DFT based on the definition given by van Rhijn (1936) is demonstrated in Table 7 with bin size of 1.00 mag, a plot of LF appears in Figure 4. Clearly, LF slopes sharply by an absolute magnitude of about  $M_G = 0.50$ -3.50 mag, LF has a constant density when  $M_G$  ranges between 3.50 and 5.00 mag, and finally, LF posses slight depression around  $M_G \sim 7$  mag which may be called a Wielen dip (Wielen, 1974).

The H-peak (or H-maximum) and R-peak (or R-maximum) in the LF are two time-dependent features (Piskunov & Belikov, 1996; Piskunov, Belikov, Kharchenko, Sagar, & Subramaniam, 2004) that discussed in LF of a coevally forming population of stars, where the lower mass stars are still in the pre-main sequence (PMS) phase and the more massive ones have already reached the main sequence (MS). They reported the arrival of stars on the MS is linked to the H-peak, which is situated at the brighter end of the LF, the peak associated with a shift in the slope of the mass-luminosity relation (MLR), which results in an identified peak in the stellar density at a particular luminosity. An evolution as a function of time, makes H-peak moves to the fainter end and therefore it is an indirect method for estimating the age of a region or population (Guo et al., 2021).

Referring to Figure 4 for analyzing H-peak in region of ( $-2.50 \leq M_G \leq -1.50$ ), Wielen dip proposed by (Lee & Sung, 1995; Lee, Sung, & Cho, 1997) at  $M_G \sim 7$ , and the R-peak at ( $7.00 \leq M_G \leq 9.50$ ), by evaluating the dispersion of whole LF and also those around H-peak, Wielen dip, and

**TABLE 6** The DFT of USC and Oph.

Magnitude (abs.)	Distance (pc)									
	80-90	90-100	100-110	110-120	120-130	130-140	140-150	150-160	160-170	170-180
-4.00 - -3.00			1		2	2	1			
-3.00 - -2.00				1		3	3	1		
-2.00 - -1.00	1					2	3	2		
-1.00 - 0.00			3	1		4	6	4	1	
0.00 - 1.00			2	1	2	8	2	3		
1.00 - 2.00			2	2	2	7	9	9	2	
2.00 - 3.00			2		1	23	29	12	2	
3.00 - 4.00			1		3	51	49	24	9	
4.00 - 5.00			2	3	6	46	44	37	7	
5.00 - 6.00			6	4	2	31	42	33	7	2
6.00 - 7.00	1		1	2	4	19	28	14	2	
7.00 - 8.00			1		1	3	11	7	2	
8.00 - 9.00									1	
9.00 - 10.00						1				

**TABLE 7** The LF of USC and Oph utilizing van Rhijn (1936) method.

$M_G$	-3.50	-2.50	-1.50	-0.50	0.50
$\log \phi(M_G)$	-5.716	-5.357	-5.391	-5.076	-5.081
$M_G$	1.50	2.50	3.50	4.50	5.50
$\log \phi(M_G)$	-4.864	-4.570	-4.271	-4.242	-4.295
$M_G$	6.50	7.50	8.50	9.50	
$\log \phi(M_G)$	-4.535	-5.018	-6.137	-6.360	

R-peak. The obtained results are about 0.674 for the whole LF, 0.024, 0.341, and 0.822 for H-peak, Wielen region, and R-peak, respectively. Therefore, the H-peak, Wielen dip, and R-peak are smoothed out in DR3 where the dispersion around them is either much smaller or slightly larger than whole LF.

LF is defined as the total number of stars per unit magnitude per unit area for non-van Rhijn (van Rhijn, 1936) scheme. Accordingly, the LF of stars in the Solar neighborhood within 20 pc from three catalogs using the same bin size of 1.00 mag as in Wielen Wielen (1974), who relied on the 1969 edition of the Gliese catalog (see (Gliese, 1969, 2015; Gliese & Jahreiß, 1991)). Once more, the second reduction is within 20 pc of the Hipparcos catalog (HIP2, van Leeuwen (2007)), and the third is built using Gaia DR2, where the peak of the LF within 20 pc is around  $M_G \approx 11$  mag. According to Guo et al. (2021) analysis using kernel density estimation (KDE), the peak at  $M_G \approx 6$  and the Wielen dip in the Gliese's curves of HIP2 remain present, while all features in the Gaia sample are smoothed out. The Wielen dip of the HIP2 and Gaia samples at  $M_G = 5$  is soothed out.

The out comes LF features showing slightly difference between these two methods based on area, volume, and distances. Therefore, these reflect on their analysis and the results as mentioned above.

The present-day mass function (PDMF) [ $\phi(\log \mathfrak{M})$ ] is defined as the number of MS stars per unit logarithmic mass interval per square parsec. The PDMF of MS field stars is related to the LF  $\phi(M_G)$  of field stars by Miller and Scalo

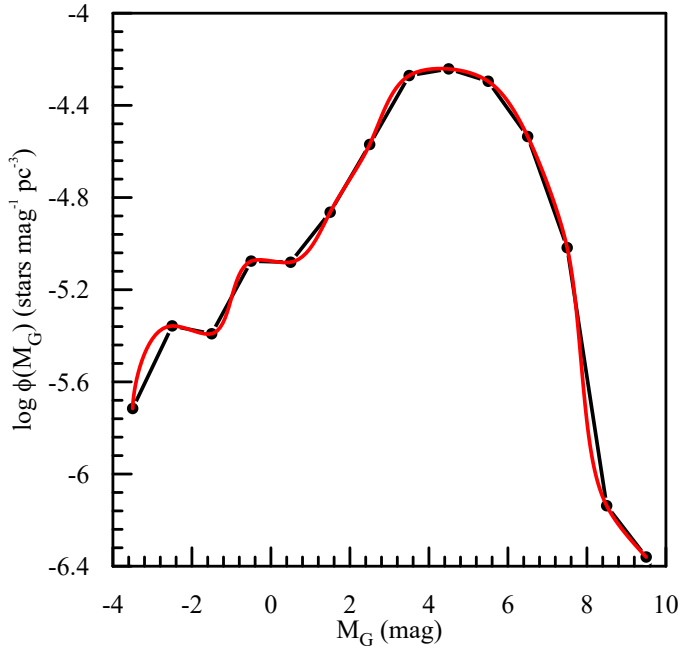


**FIGURE 4** LF and its fitted (red solid line) of the USC and Oph associations.

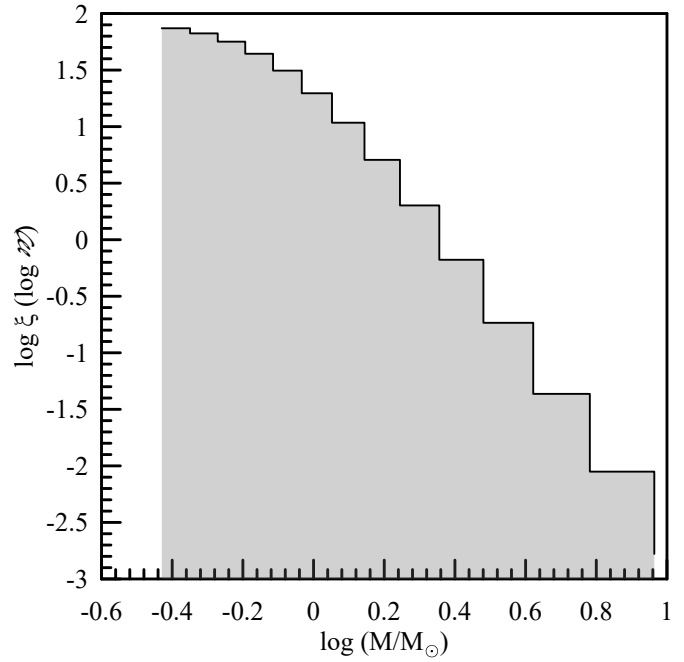


**FIGURE 5** The IMF of the present study of the USC and Oph associations.

(1979) as

$$\phi(\log \mathfrak{M}) = \phi(M_V) \left| \frac{dM_V}{d\log \mathfrak{M}} \right| 2H(M_V) f(M_V). \quad (25)$$

To produce PDMF, the visual ( $V$ ) magnitude with the provided ( $G - V$ ) color index to the  $G$ -band magnitude in DR3 according to the recipe in Riello et al. (2021), so that PDMF is in  $M_G$ . LF is converted to MF by  $dM_V/d\log \mathfrak{M}$  which is the scale with the absolute value of the derivative of the MLR (Guo et al., 2021). When LF is integrated perpendicular to the Galaxy's plane, assuming an exponential distribution with scale height  $H(M_G)$ , the result is the term  $2H(M_G)$ . According to Miller and Scalo (1979), the fraction of objects at a particular magnitude is indicated by the factor  $f(M_G)$ . The MS today (i.e.,  $T_0$ ) will contain stars with MS lifetimes ( $T_{ms}$ ) larger than the Galaxy's age, independent of their formation time. These stars have an identical PDMF [ $\phi(\log \mathfrak{M})$ ] and IMF [ $\xi(\log \mathfrak{M})$ ] (Jeřábková et al., 2018; Lee et al., 1997; Miller & Scalo, 1979; Pang et al., 2024):

$$\phi(\log \mathfrak{M}) = \xi(\log \mathfrak{M}), \quad T_{ms} \geq T_0. \quad (26)$$

To compute IMF of USC and Oph associations, referring to Eq. (25) with adopted relationship (Miller & Scalo, 1979) the obtained results are drawn here in Table 8 and the retrieved plot in Figure 5. For analyzing H-peak in regions of ( $6.053 \geq \frac{M}{M_\odot} \geq 4.188$ ), Wielen dip proposed by (Lee & Sung, 1995; Lee et al., 1997) at  $M \simeq 0.586M_\odot$ , and the R-peak within ( $0.586 \geq \frac{M}{M_\odot} \geq 0.372$ ) by evaluating the dispersion of whole

**TABLE 8** The USC and Oph associations IMF.

$M_G$	$\log(M/M_\odot)$	$\log \xi(\log \mathfrak{M})$
-3.50	0.964	-2.779
-2.50	0.782	-2.051
-1.50	0.622	-1.363
-0.50	0.481	-0.735
0.50	0.356	-0.178
1.50	0.244	0.303
2.50	0.144	0.706
3.50	0.052	1.035
4.50	-0.033	1.295
5.50	-0.115	1.495
6.50	-0.193	1.644
7.50	-0.271	1.751
8.50	-0.349	1.824
9.50	-0.430	1.870

IMF and also those around H-peak, Wielen dip, and R-peak. Therefore, the dispersion are about 1.541 for the whole IMF, 0.486, 0.076, and 0.060 for H-peak, Wielen region, and R-peak, respectively. Clearly, H & R peaks and Wielen dip are smoothed out in DR3 where dispersion around all remains much smaller than those obtained for the whole IMF. This confirmation and conclusion is compatible with those reported in Elsanhoury, Hamdy, Nouh, Saad, and Saad (2011) and recently with Gaia DR2 (Guo et al., 2021).

## 6 | DISCUSSION AND CONCLUSION

For adopted three Programs of Upper Scorpius associations. The computed kinematics, velocity ellipsoid, Solar elements, convergent points, Oort's constants, and luminosity and mass functions are studied and analyzed using the most precise three-dimensional map of our Galaxy provided by Gaia DR3.

For the first Program, the row data of  $U$ ,  $V$ , and  $W$  are extracted within Galli et al. (2018) for kinematic analysis purposes and then updated using DR3 to get about 51 Upper Scorpius stars as listed in Table 1. Program II was developed using DR2 (Gaia Collaboration et al., 2018) and new spectroscopy members of Upper Scorpius (Luhman et al., 2018). Moreover, the retrieved data are also updated with DR3 to get about two subgroups; K-type (59 stars) and M-type (83 stars) as numerated in Table 2. Third Program is devoted to seven groups (Miret-Roig, Galli, et al., 2022) in the USC and Oph associations, and the retrieved data are about 670 stars with Gaia DR3 as seen in Table 3.

Developing our code to compute kinematical parameters and the obtained conclusions are drawn here in Table 4 for Programs I, II, and III and their subgroups, into which mean space velocities ( $\overline{V}_x, \overline{V}_y, \overline{W}_z$ ; km s<sup>-1</sup>) and spatial velocities ( $\overline{U}, \overline{V}, \overline{W}$ ; km s<sup>-1</sup>) due to equatorial and Galactic coordinates, respectively are presented, velocities dispersion ( $\sigma_1, \sigma_2, \sigma_3$ ; km s<sup>-1</sup>), Solar elements ( $S_\odot$ ; km s<sup>-1</sup>) & ( $l_A^o, b_A^o, \alpha_A^o, \delta_A^o$ ), and the convergent points ( $A_o, D_o$ )<sup>o</sup>. Table 5 gives a comparison of the present study and other recent ones of ratios ( $\sigma_2/\sigma_1$ ) and Oort's constants ( $A, B$ ; km s<sup>-1</sup> kpc<sup>-1</sup>).

The density distribution in a specific direction of the Galactic plane may be deduced by the total number of stars per unit volume between absolute magnitudes  $M_G$  and  $M_G + dM_G$ , well-defined as luminosity function (van Rhijn, 1936). On the other hand, the ability to turn the luminosity function into the mass function is particularly significant, and the related initial mass functions may be analyzed due to the simple integration of evolutionary effects.

The following conclusions are obtained:

- Computed mean spatial velocities ( $\overline{U}, \overline{V}, \overline{W}$ ; km s<sup>-1</sup>) for USC as follows;  $-7.21 \pm 2.69, -16.17 \pm 4.02, -7.29 \pm 2.70$  (Program I),  $-5.25 \pm 2.29, -15.98 \pm 4.00, -7.42 \pm 2.72$  (Program II), and  $-5.05 \pm 2.25, -16.27 \pm 4.03, -7.23 \pm 2.69$  (Program III). These values are in line with those computed ones (e.g., Galli et al. (2018), Miret-Roig, Galli, et al. (2022), (Luhman & Esplin, 2020), and Wright and Mamajek (2018)).
- Mean velocities dispersion ( $\overline{\sigma}_1, \overline{\sigma}_2, \overline{\sigma}_3$ ; km s<sup>-1</sup>) for the three Programs are as follows;  $19.60 \pm 4.43, 10.41 \pm 3.23, 1.63 \pm 0.78$  (Program I),  $18.30 \pm 4.23, 2.60 \pm 0.62, 1.17$

$\pm 0.93$  (Program II), and  $1.36 \pm 0.02, 0.80 \pm 0.01, 0.96 \pm 0.01$  (Program III).

- Here, the mean Solar velocities ( $\overline{S}_\odot$ ; km s<sup>-1</sup>) are about  $19.14 \pm 4.37, 18.39 \pm 4.29, 18.62 \pm 4.32$  in unite (km s<sup>-1</sup>) of Program I, II, and III, respectively. Other Solar elements ( $l_A, b_A, \alpha_A, \delta_A$ ) numerically are listed in Table 4.
- Convergent points ( $A_o, D_o$ )<sup>o</sup> are as follows;  $94^\circ.21 \pm 0^\circ.11, -38^\circ.43 \pm 0^\circ.02$  (Program I),  $94^\circ.35 \pm 0^\circ.11, -46^\circ.50 \pm 0^\circ.15$  (Program II), and  $95^\circ.91 \pm 0^\circ.10, -44^\circ.42 \pm 0^\circ.15$  (Program III). These obtained results are confirmed with recent ones (e.g., de Bruijne (1999); Galli et al. (2018)) and Wright and Mamajek (2018) by Jones method (Jones, 1971).
- Computation the rotational constants are based on velocities dispersion ratio ( $\sigma_2/\sigma_1$ ) and the devoted results are appears in Table 5. Here, the adopted mean values of the Oort constant are about  $A = 17.80 \pm 0.24$  km s<sup>-1</sup> kpc<sup>-1</sup> and  $B = -9.61 \pm 0.32$  km s<sup>-1</sup> kpc<sup>-1</sup>. These values are consistency with other results. Notably, the selection of kinematic model characteristics may be influenced by the over or underestimation of  $A, B$ , and other dependent parameters (Hanson, 1987; Lewis, 1990). A detailed summary of all kinematical structure parameters is presented in Table 5.
- Hunting DR3 data of USC and Oph associations and their distribution to examine their luminosity function (van Rhijn, 1936) and its relation to the initial mass functions. Concluded that the obtained dispersion around three regions for H-peak, Wielen dip, and R-peak are either smaller or larger than those dispersion around whole luminosity and initial mass functions, This makes us and others on the side of an absence of these regions in OB young associations. These obtained results are compatible and confirmed by Elsanhoury et al. (2011) and in Gaia DR2 (Guo et al., 2021).

## ACKNOWLEDGMENTS

We sincerely thank the anonymous referee for their valuable suggestions, which greatly enhanced the quality of this paper. This work presents results from the European Space Agency space mission Gaia. Gaia data are being processed by the Gaia Data Processing and Analysis Consortium (DPAC). Funding for the DPAC is provided by national institutions, in particular, the institutions participating in the Gaia MultiLateral Agreement (MLA). The Gaia mission website is <https://www.cosmos.esa.int/gaia>. The Gaia archive

website is <https://archives.esac.esa.int/gaia>. The author extend their appreciation to the Deanship of Scientific Research at Northern Border University, Arar, KSA for funding this research work through the project number "NBU-FFR-2025-237-02".

## Conflict of interest

The authors declare no financial or commercial conflict of interest.

## ORCID

Waleed H. Elsanhoury <https://orcid.org/0000-0002-2298-4026>

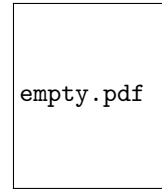
## REFERENCES

- Altmann, M., Roeser, S., Demleitner, M., Bastian, U., & Schilbach, E. (2017, April), *A&A*, 600, L4. doi:
- Ambartsumian, V. A. 1947, The evolution of stars and astrophysics. Ambartsumian, V. A. (1949, January), *AZh*, 26, 3.
- Barenfeld, S. A., Carpenter, J. M., Ricci, L., & Isella, A. (2016, August), *ApJ*, 827(2), 142. doi:
- Bessell, M. S., & Stringfellow, G. S. (1993, January), *ARA&A*, 31, 433-471. doi:
- Bisht, D., Elsanhoury, W. H., Zhu, Q. et al. (2020, September), *AJ*, 160(3), 119. doi:
- Blaauw, A. (1964, January), *ARA&A*, 2, 213. doi:
- Bland-Hawthorn, J., Sharma, S., Tepper-Garcia, T. et al. (2019, June), *MNRAS*, 486(1), 1167-1191. doi:
- Bobylev, V. V., & Bajkova, A. T. (2019, September), *Astronomy Letters*, 45(9), 580-592. doi:
- Bobylev, V. V., Bajkova, A. T., & Gromov, A. O. (2017, April), *Astronomy Letters*, 43(4), 241-251. doi:
- Bok, B. J. (1934, February), *Harvard College Observatory Circular*, 384, 1-41.
- Chupina, N. V., Reva, V. G., & Vereshchagin, S. V. (2001, May), *A&A*, 371, 115-122. doi:
- Chupina, N. V., Reva, V. G., & Vereshchagin, S. V. (2006, June), *A&A*, 451(3), 909-916. doi:
- Damiani, F., Prisinzano, L., Pillitteri, I., Micela, G., & Sciortino, S. (2019, March), *A&A*, 623, A112. doi:
- de Bruijne, J. H. J. (1999, June), *MNRAS*, 306(2), 381-393. doi:
- de Zeeuw, P. T., Hoogerwerf, R., de Bruijne, J. H. J., Brown, A. G. A., & Blaauw, A. (1999, January), *AJ*, 117(1), 354-399. doi:
- Elsanhoury, W. H. (2016, June), *Astrophysics*, 59(2), 246-255. doi:
- Elsanhoury, W. H. (2021, October), *Journal of Astrophysics and Astronomy*, 42(2), 90. doi:
- Elsanhoury, W. H. (2024, November), *New A*, 112, 102258. doi:
- Elsanhoury, W. H., & Al-Johani, A. S. (2023, September), *Astronomische Nachrichten*, 344(7), e20230047. doi:
- Elsanhoury, W. H., Hamdy, M. A., Nouh, M. I., Saad, A. S., & Saad, S. M. (2011, January), *ISRN Astronomy and Astrophysics*, 2011, 127030. doi:
- Elsanhoury, W. H., Nouh, M. I., & Abdel-Rahman, H. I. (2015, October), *Rev. Mexicana Astron. Astrofis.*, 51, 199. doi:
- Elsanhoury, W. H., Nouh, M. I., Branham, R. L., & Al-Johani, A. S. (2021, August), *Astronomische Nachrichten*, 342(989), 989-998. doi:
- Elsanhoury, W. H., Postnikova, E. S., Chupina, N. V., Vereshchagin, S. V., Sariya, D. P., Yadav, R. K. S., & Jiang, I.-G. (2018, March), *Ap&SS*, 363(3), 58. doi:
- Esplin, T. L., Luhman, K. L., Miller, E. B., & Mamajek, E. E. (2018, August), *AJ*, 156(2), 75. doi:
- Gaia Collaboration. (2022, May), *VizieR Online Data Catalog*, I/355.
- Gaia Collaboration, Brown, A. G. A., Vallenari, A. et al. (2018, August), *A&A*, 616, A1. doi:
- Gaia Collaboration, Brown, A. G. A., Vallenari, A. et al. (2021, May), *A&A*, 649, A1. doi:
- Gaia Collaboration, Prusti, T., de Bruijne, J. H. J. et al. (2016, November), *A&A*, 595, A1. doi:
- Gaia Collaboration, Vallenari, A., Brown, A. G. A. et al. (2023, June), *A&A*, 674, A1. doi:
- Galli, P. A. B., Joncour, I., & Moraux, E. (2018, June), *MNRAS*, 477(1), L50-L54. doi:
- Girard, T. M., van Altena, W. F., Zacharias, N. et al. (2011, July), *AJ*, 142(1), 15. doi:
- Gliese, W. (1969, January), *Veroeffentlichungen des Astronomischen Rechen-Instituts Heidelberg*, 22, 1.
- Gliese, W. (2015, November), *VizieR Online Data Catalog: Catalogue of Nearby Stars, Edition 1969 (Gliese, 1979)*, *VizieR On-line Data Catalog: V/1*. Originally published in: 1969VeARI..22....1G.
- Gliese, W., & Jahreiß, H. (1991, January), Preliminary Version of the Third Catalogue of Nearby Stars., On: The Astronomical Data Center CD-ROM: Selected Astronomical Catalogs, Vol. I; L.E. Brodzmann, S.E. Gesser (eds.), NASA/Astronomical Data Center, Goddard Space Flight Center, Greenbelt, MD.
- Guo, D., de Koter, A., Kaper, L., Brown, A. G. A., & de Bruijne, J. H. J. (2021, November), *A&A*, 655, A45. doi:
- Hanson, R. B. (1987, August), *AJ*, 94, 409. doi:
- Jeřábková, T., Hasani Zonoozi, A., Kroupa, P., Beccari, G., Yan, Z., Vazdekis, A., & Zhang, Z. Y. (2018, November), *A&A*, 620, A39. doi:
- Johnson, D. R. H., & Soderblom, D. R. (1987, April), *AJ*, 93, 864. doi:
- Jones, D. H. P. (1971, January), *MNRAS*, 152, 231. doi:
- Kordopatis, G., Gilmore, G., Steinmetz, M. et al. (2013, November), *AJ*, 146(5), 134. doi:
- Krisanova, O. I., Bobylev, V. V., & Bajkova, A. T. (2020, June), *Astronomy Letters*, 46(6), 370-378. doi:
- Lawrence, A., Warren, S. J., Almaini, O. et al. (2007, August), *MNRAS*, 379(4), 1599-1617. doi:
- Lee, S.-W., & Sung, H. (1995, April), *Journal of Korean Astronomical Society*, 28(1), 45-59.
- Lee, S.-W., Sung, H., & Cho, D.-H. (1997, October), *Journal of Korean Astronomical Society*, 30(2), 181-189.
- Lewis, J. R. (1990, May), *MNRAS*, 244, 247-253.
- Li, C., Zhao, G., & Yang, C. (2019, February), *ApJ*, 872(2), 205. doi:
- Lindgren, L., Lammers, U., Bastian, U. et al. (2016, November), *A&A*, 595, A4. doi:
- Liu, J. C., Zhu, Z., & Hu, B. (2011, December), *A&A*, 536, A102. doi:
- Lodieu, N., Hambly, N. C., & Jameson, R. F. (2006, November), *MNRAS*, 373(1), 95-104. doi:
- Luhman, K. L., & Esplin, T. L. (2020, July), *AJ*, 160(1), 44. doi:
- Luhman, K. L., Herrmann, K. A., Mamajek, E. E., Esplin, T. L., & Pecaut, M. J. (2018, August), *AJ*, 156(2), 76. doi:
- Luhman, K. L., & Mamajek, E. E. (2012, October), *ApJ*, 758(1), 31.

- doi:
- Luyten, W. J. (1968, January), *MNRAS*, *139*, 221. doi:
- Malo, L., Artigau, É., Doyon, R., Lafrenière, D., Albert, L., & Gagné, J. (2014, June), *ApJ*, *788*(1), 81. doi:
- Mann, A. W., Newton, E. R., Rizzuto, A. C. et al. (2016, September), *AJ*, *152*(3), 61. doi:
- Maurya, J., Joshi, Y. C., Elsanhoury, W. H., & Sharma, S. (2021, August), *AJ*, *162*(2), 64. doi:
- McCuskey, S. W. (1966, January), *Vistas in Astronomy*, *7*(1), 141-171. doi:
- Mihalas, D., & Binney, J. 1981, Galactic astronomy. Structure and kinematics.
- Miller, G. E., & Scalo, J. M. (1979, November), *ApJS*, *41*, 513. doi:
- Miret-Roig, N., Bouy, H., Raymond, S. N. et al. (2022, February), *Nature Astronomy*, *6*, 89-97. doi:
- Miret-Roig, N., Galli, P. A. B., Olivares, J., Bouy, H., Alves, J., & Barrado, D. (2022, November), *A&A*, *667*, A163. doi:
- Nouh, M. I., & Elsanhoury, W. H. (2020, June), *Astrophysics*, *63*(2), 179-189. doi:
- Oort, J. H. (1927a, October), *Bull. Astron. Inst. Netherlands*, *4*, 91.
- Oort, J. H. (1927b, April), *Bull. Astron. Inst. Netherlands*, *3*, 275.
- Pang, X., Liao, S., Li, J. et al. (2024, May), *ApJ*, *966*(2), 169. doi:
- Pecaut, M. J., & Mamajek, E. E. (2016, September), *MNRAS*, *461*(1), 794-815. doi:
- Piskunov, A. E., & Belikov, A. N. (1996, July), *Astronomy Letters*, *22*(4), 466-469.
- Piskunov, A. E., Belikov, A. N., Kharchenko, N. V., Sagar, R., & Subramaniam, A. (2004, April), *MNRAS*, *349*(4), 1449-1463. doi:
- Preibisch, T., Brown, A. G. A., Bridges, T., Guenther, E., & Zinnecker, H. (2002, July), *AJ*, *124*(1), 404-416. doi:
- Preibisch, T., & Mamajek, E. (2008), The Nearest OB Association: Scorpius-Centaurus (Sco OB2). In B. Reipurth (Ed.), *Handbook of Star Forming Regions, Volume II Vol. 5*, p. 235. doi:
- Preibisch, T., & Zinnecker, H. (1999, May), *AJ*, *117*(5), 2381-2397. doi:
- Richert, A. J. W., Getman, K. V., Feigelson, E. D. et al. (2018, July), *MNRAS*, *477*(4), 5191-5206. doi:
- Riello, M., De Angeli, F., Evans, D. W. et al. (2021, May), *A&A*, *649*, A3. doi:
- Rizzuto, A. C., Ireland, M. J., & Kraus, A. L. (2015, April), *MNRAS*, *448*(3), 2737-2748. doi:
- Rizzuto, A. C., Ireland, M. J., & Robertson, J. G. (2011, October), *MNRAS*, *416*(4), 3108-3117. doi:
- Skrutskie, M. F., Cutri, R. M., Stiening, R. et al. (2006, February), *AJ*, *131*(2), 1163-1183. doi:
- Slesnick, C. L., Carpenter, J. M., & Hillenbrand, L. A. (2006, June), *AJ*, *131*(6), 3016-3027. doi:
- Smart, W. M. 1968, Stellar kinematics.
- Song, I., Zuckerman, B., & Bessell, M. S. (2012, July), *AJ*, *144*(1), 8. doi:
- Taylor, M. B. (2005, December), TOPCAT & STIL: Starlink Table/VOTable Processing Software. In P. Shopbell, M. Britton, & R. Ebert (Eds.), *Astronomical Data Analysis Software and Systems XIV Vol. 347*, p. 29.
- Trumpler, R. J., & Weaver, H. F. 1953, Statistical astronomy.
- Tutukov, A. V., Chupina, N. V., & Vereshchagin, S. V. (2023, December), *Astronomy Reports*, *67*(12), 1418-1441. doi:
- van Leeuwen, F. 2007, Hipparcos, the New Reduction of the Raw Data (Vol. 350). doi:
- van Rhijn, P. J. (1936, January), *Publications of the Kapteyn Astronomical Laboratory Groningen*, *47*, 1-34.
- Vereshchagin, S. V., Chupina, N. V., Sariya, D. P., Yadav, R. K. S., & Kumar, B. (2014, August), *New A*, *31*, 43-50. doi:
- Žerjal, M., Ireland, M. J., Crundall, T. D., Krumholz, M. R., & Rains, A. D. (2023, March), *MNRAS*, *519*(3), 3992-4009. doi:
- Wang, F., Zhang, H. W., Huang, Y., Chen, B. Q., Wang, H. F., & Wang, C. (2021, June), *MNRAS*, *504*(1), 199-207. doi:
- Wenger, M., Ochsenein, F., Egret, D. et al. (2000, April), *A&AS*, *143*, 9-22. doi:
- Wielen, R. (1974, January), *Highlights of Astronomy*, *3*, 395-407.
- Wright, N. J., & Mamajek, E. E. (2018, May), *MNRAS*, *476*(1), 381-398. doi:
- Zacharias, N., Finch, C. T., Girard, T. M., Henden, A., Bartlett, J. L., Monet, D. G., & Zacharias, M. I. (2013, February), *AJ*, *145*(2), 44. doi:



## AUTHOR BIOGRAPHY



**Waleed H. Elsanhoury**, born in 1972 in Egypt, is a full professor at the National Research Institute of Astronomy and Astrophysics (NRIAG), located in Helwan, Cairo, Egypt. He is currently affiliated with the College of Science, Physics Department, at Northern Border University in Saudi Arabia. He earned his Ph.D. in Theoretical Physics in 2009 from Physics Department, Faculty of Science, at Al-Azhar University, Egypt. Prior to that, he received his M.Sc. in Physics in 2004 from Physics Department, Faculty of Science, at Helwan University, Egypt, and his B.Sc. in Physics (Special Degree) in 1994 from Physics Department, Faculty of Science, at Alexandria University, Egypt. His research interests focus on computational and mathematical physics, with particular emphasis on their applications in astronomy and astrophysical models, utilizing the Mathematica software package. His current research is dedicated to investigating the photometry, astrometry, dynamical evolution, and kinematic behaviors of open star clusters and their associations in the Gaia era. His body of work includes 53 publications, which have been cited approximately 178 times.

